CANADIAN JOURNAL OF EXPLORATION GEOPHYSICS
VOL. 25, NO. 1 (JUNE 1989) P. 61-73

DETECTION OF A BRINE CONDUCTOR UNDER AN OIL FIELD BY MEANS OF A FIXED TRANSMITTER ELECTROMAGNETIC SURVEY USING A SQUID MAGNETOMETER

K. DUCKWORTH[1] AND D. O'NEILL[2]

ABSTRACT

A low-frequency (1 to 15 Hz) electromagnetic survey was conducted over a brine conductor located in a sandstone lens underlying a heavy oil field. This conductor is at a depth of 780 m and displays a conductivity on drill hole logs which is comparable to the conductivity of sulphide ore bodies. This suggested that the conductor would be amenable to detection by methods developed for metallic mineral exploration. The transmitter consisted of a 6.8-km line, grounded at each end, carrying a 1-Hz, 2-amp square wave current. The resultant field was detected along a 6-km traverse which ran parallel to the transmitter line at a distance of 1.6 km. The detector was a three-component SQUID-type magnetometer. The output of the magnetometer permitted amplitude and phase of the secondary field to be derived from its elliptical characteristics. Digital acquisition of the signal permitted frequency information from 1 to 15 Hz to be extracted from the square wave signal by Fourier transformation.

The resultant total secondary-field profiles displayed a strong reflected component due to the low (5 ohm-m) resistivity of the host environment. In addition, the profiles showed localized anomalies which proved to be consistent with a source located at the known depth of the brine conductor.

INTRODUCTION

Hydrocarbon deposits are commonly associated with highly saline brine which is localized within the same structure as the hydrocarbons. An example of this type of situation is provided by the David oil field which is located 10 km northwest of the town of Provost in eastern Alberta (Figure 1). The oil is contained in a structural drape over a sandstone lens of Lower Cretaceous age which is located at a depth of 780 m and is contained within an area 3 km long by 1 km wide, as shown in Figure 2. The very conductive brine contained within this 50-m thick sandstone lens causes the sandstone to display a conductivity (1.7 S/m) which is comparable to that of many metallic mineral ore structures (Parkhomenko, 1967).

Electromagnetic surveys using fixed-loop, Turam-type transmitters are notably successful in the detection of deep localized conductors of the type commonly encountered in metallic mineral exploration (Bosschart, 1964; Jagodits et al., 1986; Duckworth, 1988). Thus, the localized character and high conductivity of the structure which controls the David oil field suggest that conductors of this type may be detectable by means of traverses conducted with fixed transmitter electromagnetic systems.

The aim of the test survey described in this paper was to examine the possibility of using such methods to detect hydrocarbon traps of the type represented by the David field.

While the high conductivity and localized character of the brine conductor below the David field make it appear to be an ideal electromagnetic target, the conductor and its environment display other features which obliged us to use unconventional adaptations of fixed transmitter methods in our attempt to detect it.

The first of these features is its depth of 780 m, which indicates that any anomalous field due to the conductor will be distributed over a distance of 3 to 4 km at the surface. Thus, the length of traverse required to fully explore such an anomaly needs to be significantly greater than 4 km. However, in fixed transmitter surveys applied to mineral deposits, the traverse length seldom exceeds 2 km. This limitation is inherent to the conventional mode of operation in which traverses are run perpendicular to the transmitter which is normally a large rectangular loop. The strong geometric attenuation of the field as distance from a loop transmitter is increased, results in the field becoming too small to be detected at ranges of 2 to 3 km unless an unreasonably large current is used in the transmitter.

An alternative mode of operation, which allows traverses to be as long as required (Duckworth and Bays, 1984), was adopted for the test survey described here. This procedure involves running the traverses parallel to the transmitter loop which is laid directly across the anticipated trend of

Manuscript received by the Editor March 10, 1989; revised manuscript received May 10, 1989.

[1]Department of Geology and Geophysics, University of Calgary, Calgary, Alberta T2N 1N4

[2]Texaco Canada Resources Ltd., 605 - 5th Ave. S.W., P.O. Box 3333 Station M, Calgary, Alberta T2P 2P8

This project was supported by a grant from the Natural Sciences and Engineering Research Council of Canada (NSERC) (grant P-8403), as well as by grants from the Imperial Oil program of grants to higher education and from PanCanadian Petroleum Ltd., the company which operates the David field. The field operations would not have been possible without the diligent and resourceful efforts of Carl Gunhold and Eric Gallant.

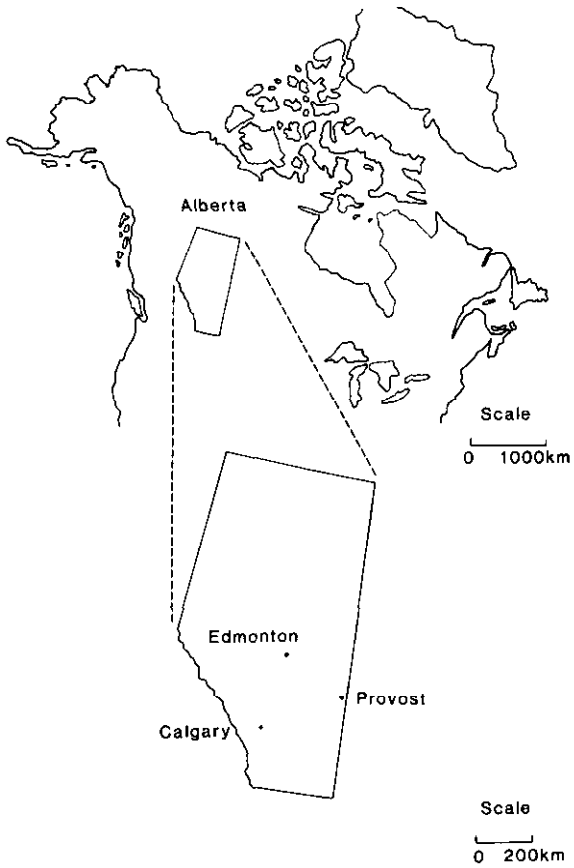

Fig. 1. Location map. The town of Provost which is located 10 km SE of the survey area.

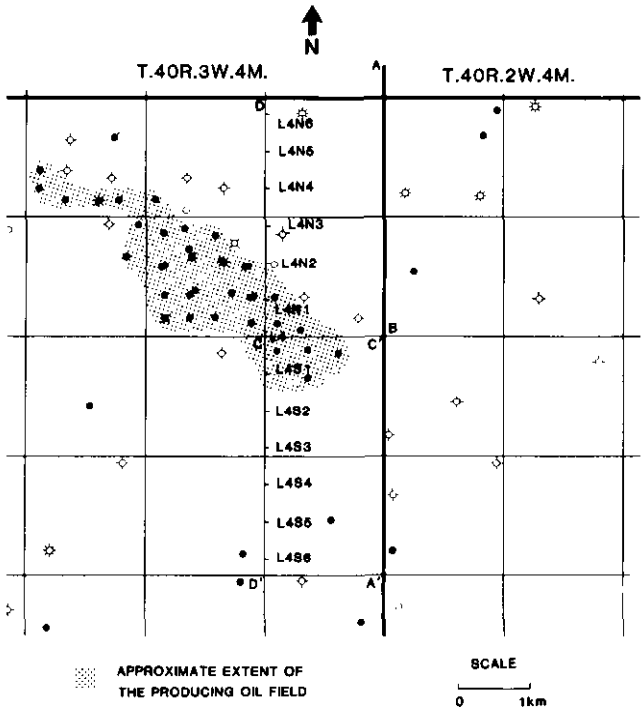

Fig. 2. The transmitter line was laid between points A and A'. Readings were taken at 500-m intervals along the traverse D to D'.

the conductor. The length of traverse depends only on the length of the transmitter loop.

This configuration provides very good inductive linkage to flat-lying conductors of the type represented by the sandstone lens under the David field, as shown by Duckworth and Cummins (1989). It also allows the transmitter current to be moderate (we used only 2 amps) while providing any desired length of traverse, which in the case of this test survey was 6 km. An additional advantage of this mode of operation is that the primary-field intensity can be made almost uniform along the traverse if the transmitter loop is made longer than the traverse line. This contrasts with the strong gradient of the primary field which exists in data acquired along lines run perpendicular to a loop transmitter. The lack of gradient in the primary field offered by the alternative procedure is a considerable aid to the recognition of subtle anomalies due to deep conductors.

A feature of the host environment which presented a special problem was the low resistivity of the rocks overlying the oil field. These are marine Cretaceous shales which, on drill logs, show an average resistivity of 5 ohm-m for the whole section down to the sandstone. In a 20-m section from 565 m to 585 m, the resistivity is as low as 2 ohm-m while the highest resistivity is 17 ohm-m between depths of 90 m and 110 m. The resistivity of the sandstone lens is 0.6 ohm-m on the logs, so that its conductivity is approximately 8 times greater than that of the overlying rocks.

Even at 20 Hz, absorption of the field in the overlying conductive rocks would cause the transmitted field experienced by the sandstone lens to be 95 percent weaker (13 dB loss) than if the overlying rocks were resistive. A similar loss would be experienced by any field emitted from this conductor in propagating to the surface. An alternative view of this situation is provided by noting that at 20 Hz the 780-m depth of the target would be 3.1 times greater than the skin depth of the conductive environment and would be equal to one skin depth for a frequency of 2.1 Hz.

These absorption losses occur in combination with the inevitable strong geometric attenuation of the field. Therefore, it appeared improbable that any appreciable field due to the conductor could be generated or detected at 20 Hz.

A frequency of 1 Hz was chosen for this test survey because it offered only 49 percent (3.1 dB) attenuation loss at the depth of the target while also being relatively free of natural electromagnetic noise, as discussed by Keller and Frischknecht (1966). At this frequency, the skin depth of the host environment was 1.4 times greater than the depth-to-target conductor. This frequency is not commonly available in electromagnetic transmitters designed for mineral surveys but is available in the generators designed for induced polarization (IP) surveys. We employed a Phoenix IPT-1 2.5 kW transmitter. The square wave output of this type of generator also allowed us to extract higher frequency information from the harmonics of the square wave up to 15 Hz.

Electromagnetic receivers designed for mineral prospecting do not cover this low-frequency range, but the detection of electromagnetic fields in the frequency range from 1 to 15 Hz is ideally suited to SQUID-type (superconducting quantum interference device) magnetometers (Zimmerman and Campbell, 1975). These devices readily provide a sensitivity of 10^{-4} nT while also offering separate detectors for the vertical and the two horizontal components of the detected field within the same instrument. SQUID instruments present special operational demands because of the large volume of liquid helium that must be provided to keep the sensor in the superconducting state for a reasonable period of operation in the field. The unit we employed was a CTF DSQ/RFM-400 with a 30-litre cryostat (Figure 3) which allowed 10 days of field operation without reloading, although we did develop the means to reload the cryostat in the field.

Another operational problem is the need to isolate the detector when taking readings. It was necessary to locate the magnetometer 100 m from the recording system and associated generators. However, a similar separation from a coil-type receiver system would be needed if it matched the sensitivity of the SQUID detector over this same 1 to 15 Hz frequency range. A further problem when working at low frequency is the need to protect the detector from wind-induced vibration, which causes spurious signal due to the variation of the coupling of the detector with the Earth's magnetic field. This protection can be provided by partially burying the magnetometer, but we used a wooden shield as shown in Figure 3. The shield is shown with one wall removed. It permitted frequent movement of the magnetometer to new stations without the need to dig holes. The shield was firmly anchored to the ground after the magnetometer had been levelled on its base plate.

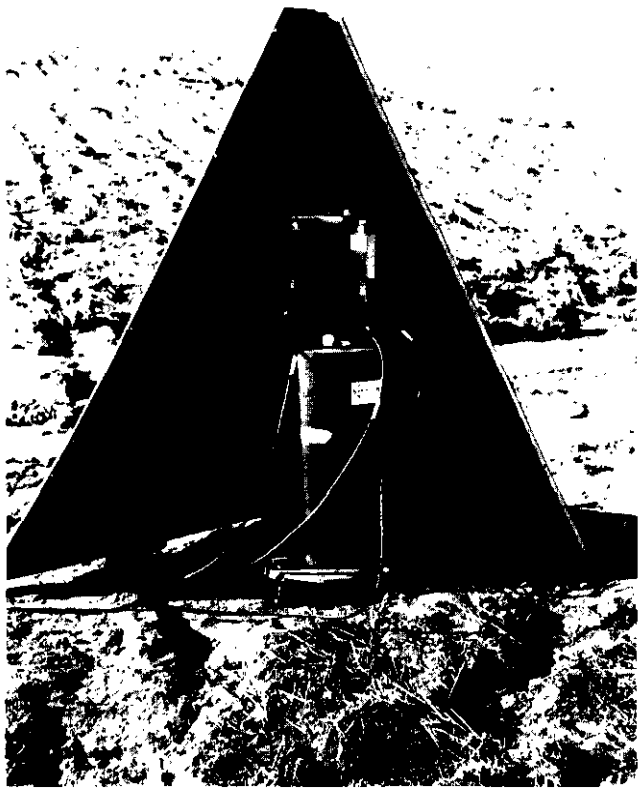

Fig. 3. The CTF Systems DSQ/RFM-400 three-component magnetometer holds 30 litres of liquid helium for 10 days of operation. The wooden shield prevented wind-induced noise.

Thus, the brine underlying the David oil field appeared to present a target suitable for detection by means of a fixed transmitter electromagnetic survey and it appeared that appropriate equipment and procedures were available to allow such a survey to be conducted.

Survey Procedure

A large rectangular loop transmitter with a total length of 19.2 km laid along available roads was initially planned. However, encounters with farm machinery made it clear that a loop of this length would be hard to maintain in view of the numerous roads and farm entries which it would cross. We therefore minimized this problem by using a grounded-line type of transmitter located where the front edge of the loop transmitter had been planned. The low resistivity of the ground in the test area allowed the generator to deliver 2 amps consistently through the 6.8 km of 16 gauge insulated copper wire between the grounding points.

The transmitter wire was laid, as shown in Figure 2, along the north-south line denoted AA′ which was located to the east of the oil field. The parallel survey line denoted DD′ passed through the oil field and was located 1.6 km to the west of the transmitter. Stations on this line were placed at 500 m intervals. The line CC′ was used for development tests and for easy access to the transmitter generator located at point B.

Data Acquisition and Treatment

An example of a record taken from one of the survey stations is shown in Figure 4. The channel 0 horizontal-component sensor was decoupled from the field by careful orientation of the instrumentation before the reading was taken. This was done at each station.

The record shown in Figure 4 was the result of a 20-fold stack of two complete cycles of the recorded signal. Each trace consists of 256 discrete, digitally acquired samples which have been joined by a linear interpolator for display purposes. Stacking was achieved by transferring the digital output of the DSQ-400 to an IBM-PC computer by direct memory access. Triggering was controlled by a crystal clock which duplicated the period of the clock driving the transmitter. Relative drift between these two clocks was no more than 0.9 microseconds in any 24-hour period.

Because of the quantization of magnetic flux which is an inherent feature of a SQUID magnetometer, it is able to provide a dynamic range of 193 dB with no loss of accuracy throughout the range (Vrba et al., 1981). It counts changes in the number of flux quanta linked with the sensor but is also able to measure changes as small as 10^{-4} of a single

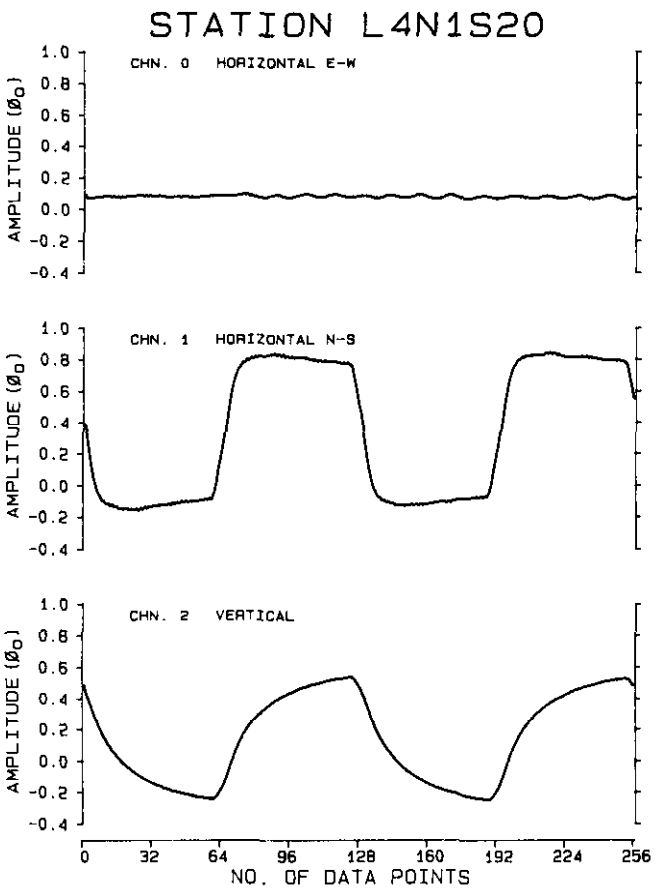

Fig. 4. A typical record from the magnetometer. Signal magnitude was approximately 1 nT. Units are Flux Quanta where one Flux Quantum was approximately 1 nT for this magnetometer. The E-W horizontal component sensor was decoupled from the field by careful orientation of the instrument.

flux quantum, where one quantum (denoted ϕ_0) is given by

$$\phi_0 = h/(2.e) = 2.07 \times 10^{-15} \text{ Webers},$$

where e is the charge on an electron and h is Plank's constant.

For the instrument we were using, the calibration factors for conversion of flux quanta to magnetic field were

$\phi_0 = 0.79$ nT horizontal

$\phi_0 = 1.05$ nT vertical.

The difference between these values reflects the difference between the flux transformers which are interposed between the field being sampled and the separate SQUID device devoted to each channel.

Thus, with the system able to detect changes of $10^{-4}\ \phi_0$, this gave a sensitivity of approximately 10^{-4} nT (i.e., 10^{-4} gamma) for both vertical and horizontal components.

The records for all three components of the field were acquired simultaneously to permit phase differences between the components to be determined. After stacking, the recorded signals were stored on disc. Subsequently, each record was Fourier transformed into its harmonic components, so that, for each station, the magnitudes of the vertical (**V**) and horizontal (**H**) vector components and the phase difference between these two components were calculated for frequencies of 1, 3, 5, 7, 9, 11, 13 and 15 Hz.

These values of **V** and **H** and their relative phase at each station were then combined with the calculated magnitude of the primary field (**P**) at each station to permit the magnitude of the equivalent secondary field (**S**) at each station to be computed. This process also permitted the spatial direction and absolute phase of the equivalent secondary field with respect to the transmitter to be determined. This overall reduction process is embodied in Figure 5 which shows the polarization ellipse generated by the recorded **V** and **H** vectors. This recorded polarization ellipse can be treated as being the result of the interaction of the vertically oriented primary field **P** and the resultant secondary field which is represented by an equivalent vector **S**. It must be noted that **S** is not the actual secondary field, as discussed later.

The derivation of **S** was handled by a computer algorithm which performed a process which was equivalent to constructing the parallelogram ABCD in Figure 5, which

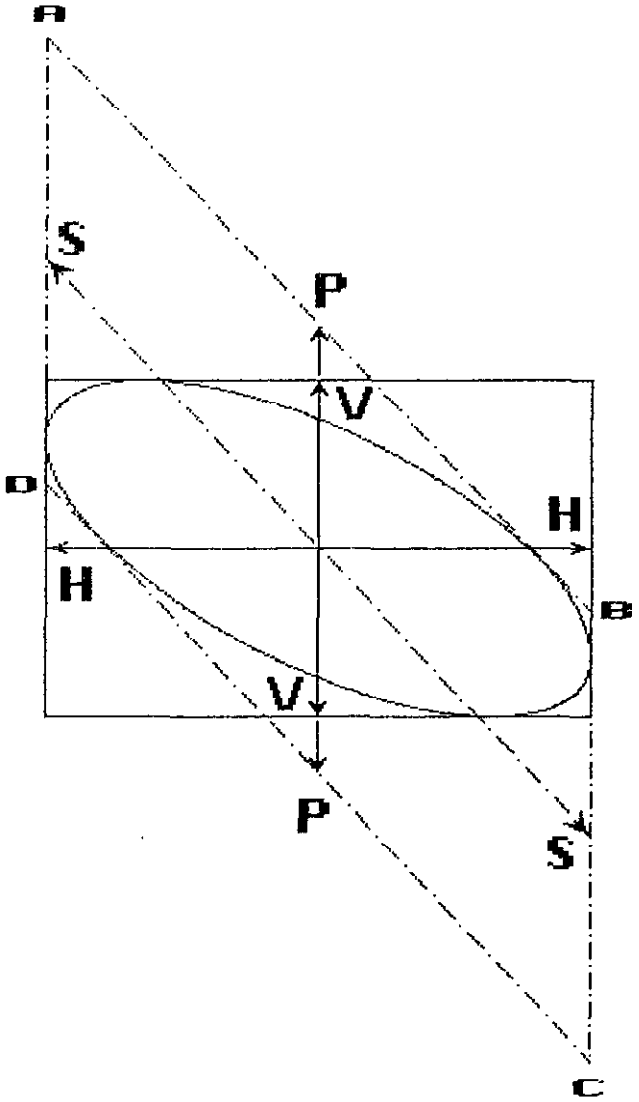

Fig. 5. The recorded field components **V** and **H** produced an ellipse of polarization which permitted the equivalent secondary field **S** to be derived, given the known magnitude of the transmitted field **P**.

contained the known ellipse, the known vector **P** and the unknown vector **S** as shown. This process constrained the spatial direction and magnitude of the vector **S**. The phase relationships of the vectors are embodied in the points at which the ellipse touches the parallelograms which contain each pair of vectors. In the case shown, the phase difference between **V** and **H** was approximately 50 degrees while that between **P** and **S** was approximately 130 degrees. This is difficult to appreciate visually because phase is not linearly distributed along the axes represented by the parallelograms.

If the secondary field at the station had been generated by a single isolated source, then that field would have been a linearly polarized field. However, when more than one source of secondary field is present, as was certainly the case for these results, then the secondary field will itself be elliptically polarized unless all the sources of secondary field are in phase, which is physically improbable. The vector, **S**, which was generated by the process described above, was a linearly polarized vector, yet it represented a secondary field which was inevitably elliptically polarized. Thus, it is necessary to refer to **S** as the linear equivalent secondary field. The essential property of **S** is that its vertical and horizontal components are identical to the vertical and horizontal components of the actual elliptically polarized secondary field.

Profiles of **S** for the 8 frequencies extracted from the 1-Hz square wave field are shown in Figures 6 to 9. The discrete data points represent the data obtained from the field records. The solid-line profiles matched to the amplitude data were generated by means of theoretical modelling.

Results

The main feature of the profiles presented in Figures 6 to 9 is the arched form displayed by the amplitude of the secondary field. This is most easily seen in the 13- and 15-Hz data of Figure 9. This feature was also a characteristic of the primary field **P**, which inevitably weakened as the traverse approached the ends of the transmitter line at the northern and southern ends of the traverse. Thus, the arch in the secondary-field profiles can be understood as being due to a reflected image of the transmitted field created by inductive interaction between the primary field and the very conductive environment.

In addition to this image of the transmitter field, there are localized secondary-field anomalies with magnitudes of the order of 0.1 nT which are most easily seen in the profiles for 5, 7, 9 and 11 Hz. The 3 to 4 km lateral extent of each of these anomalies appears to be consistent with sources located at the 780-m depth of the brine conductor. It is notable that these localized anomalies fade out at higher frequencies, leaving only the secondary field due to the overall environment. This appears to confirm that, at these higher frequencies, fields from the brine conductor could not reach the surface with sufficient magnitude to be detectable.

Absolute confirmation that the brine conductor is the source of these localized anomalies is not possible when only one traverse is available. However, it is possible to establish that the anomalies are compatible with this concept by matching the observed data with data generated by a theoretical model constrained to place the source of this localized secondary field at the known depth of the brine conductor.

In the situation presented by the David oil field, several possible sources of concentrations of current within the brine must be considered. The first of these is the directly induced current due to the inductive interaction between the conductor and the magnetic field emitted by the current-carrying transmitter line. The second is the gathering into the conductor of the return (galvanic) current between the grounding points for the transmitter line. The third is the gathering into the brine conductor of current induced into the conductive host by the field from the transmitter line, as shown by Lajoie and West (1976). A fourth consideration (Duckworth and Cummins, 1989) is that if more than one localized conductor is present in the area, then the fields emitted by the currents which are generated within each conductor must influence all other conductors.

All of these effects can be treated fully only in a three-dimensional theoretical model. Such models require extensive computing power, but a simple alternative is available which can be implemented on any personal computer (Duckworth, 1972, 1988; Duckworth and O'Neill, 1989). This alternative method simulates the observed field by computing the vector characteristics of the field due to a grouping of hypothetical, subsurface, horizontal line current elements. The position, magnitude and phase of each current element within a simulated section of the target area are controlled by iterative matching of the total synthetic line current field to the observed field. It was shown by Duckworth and O'Neill (1989) that the positions adopted by the currents derived by this process correspond well to the actual spatial locations of the target conductors, both laterally and in depth, even when those target conductors are located in a very conductive host. However, this process does not attempt to provide the actual current magnitudes and phases which existed within the conductors.

The matching amplitude profiles, shown as solid lines in Figures 6 to 9, were generated by this simple model. The line current elements which generated the match to the localized anomalies are shown in the section below each profile. These current elements were constrained to lie at the same 780-m depth for all frequencies. The arched profile in the amplitude data was simulated by means of a line current oriented parallel to the traverse line so that this particular current does not appear on the cross-section below each profile.

The match to the observed amplitude data is particularly effective at 9 Hz (Figure 8), but at lower frequencies the increased noise level prevented a good match from being achieved. The phase profiles also appear to contain localized anomalies which correspond to the amplitude anoma-

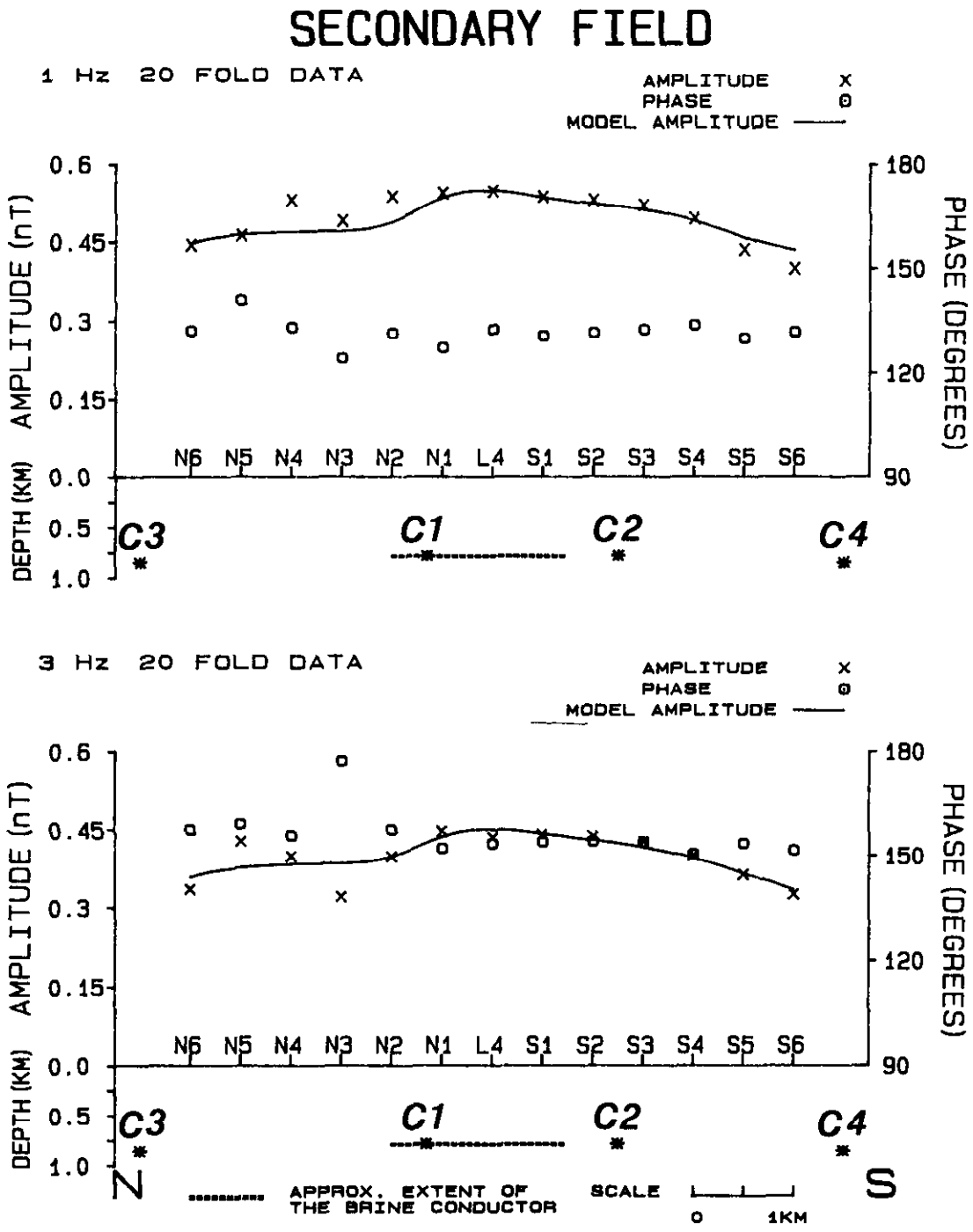

Fig. 6. Profiles of total secondary field obtained at 1 Hz and 3 Hz. The solid profiles were generated by a theoretical line-current model. The positions of the currents used in this model are shown in the section below the profile along with the approximate extent of the oil field.

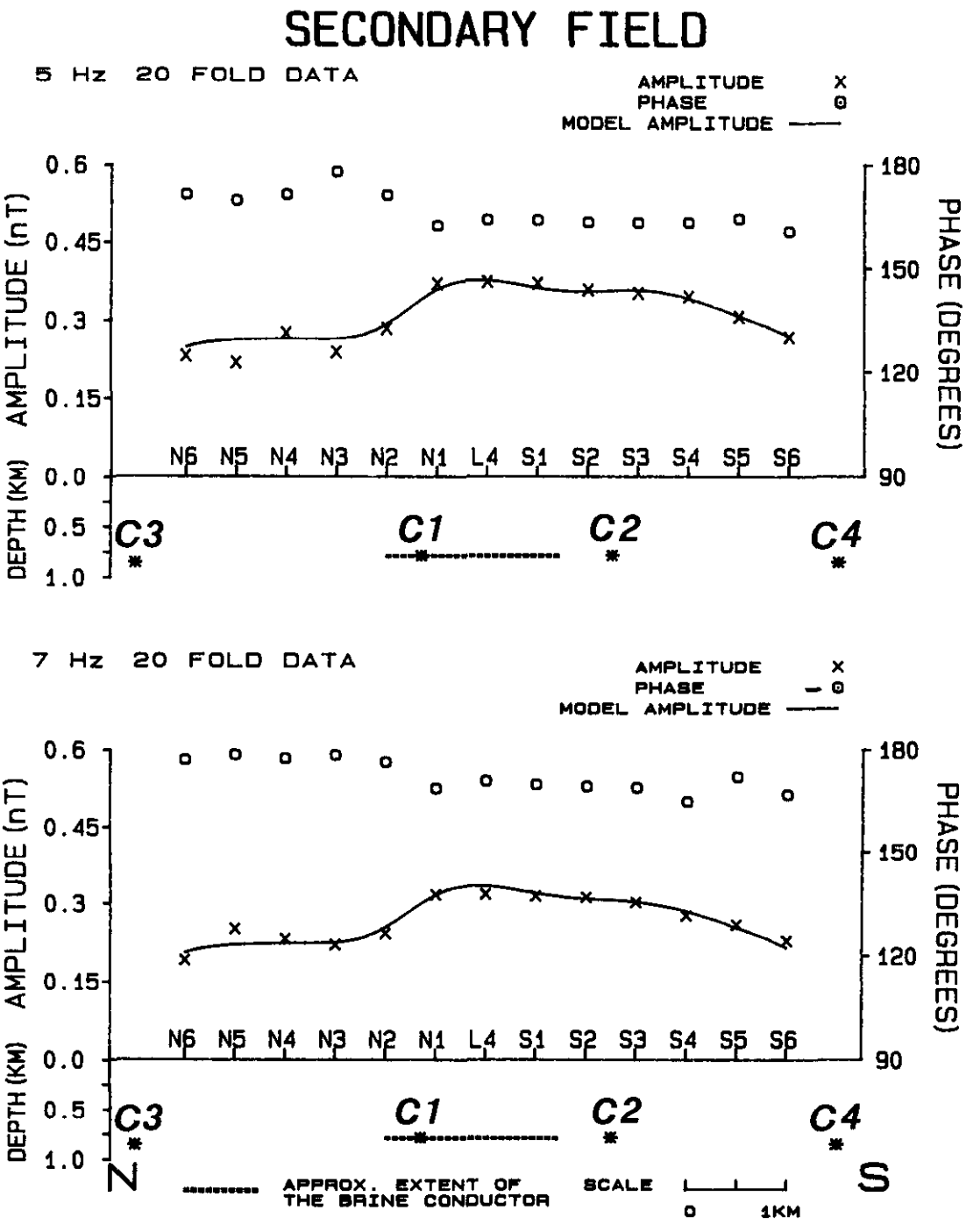

Fig. 7. Localized anomalies with lateral extents of 3 to 4 km and magnitudes of approximately 0.1 nT are evident in these profiles for 5 and 7 Hz.

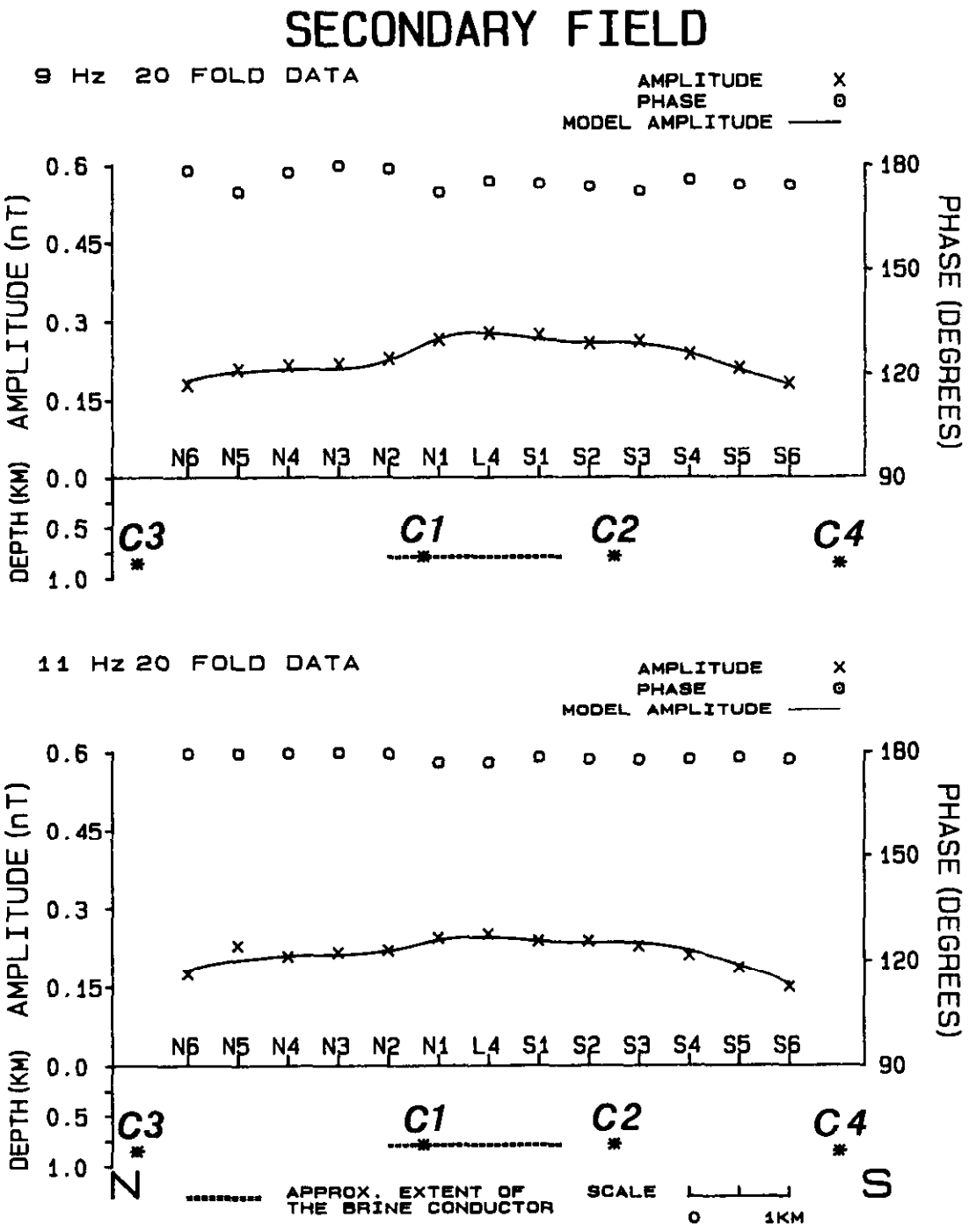

Fig. 8. The 9- and 11-Hz profiles.

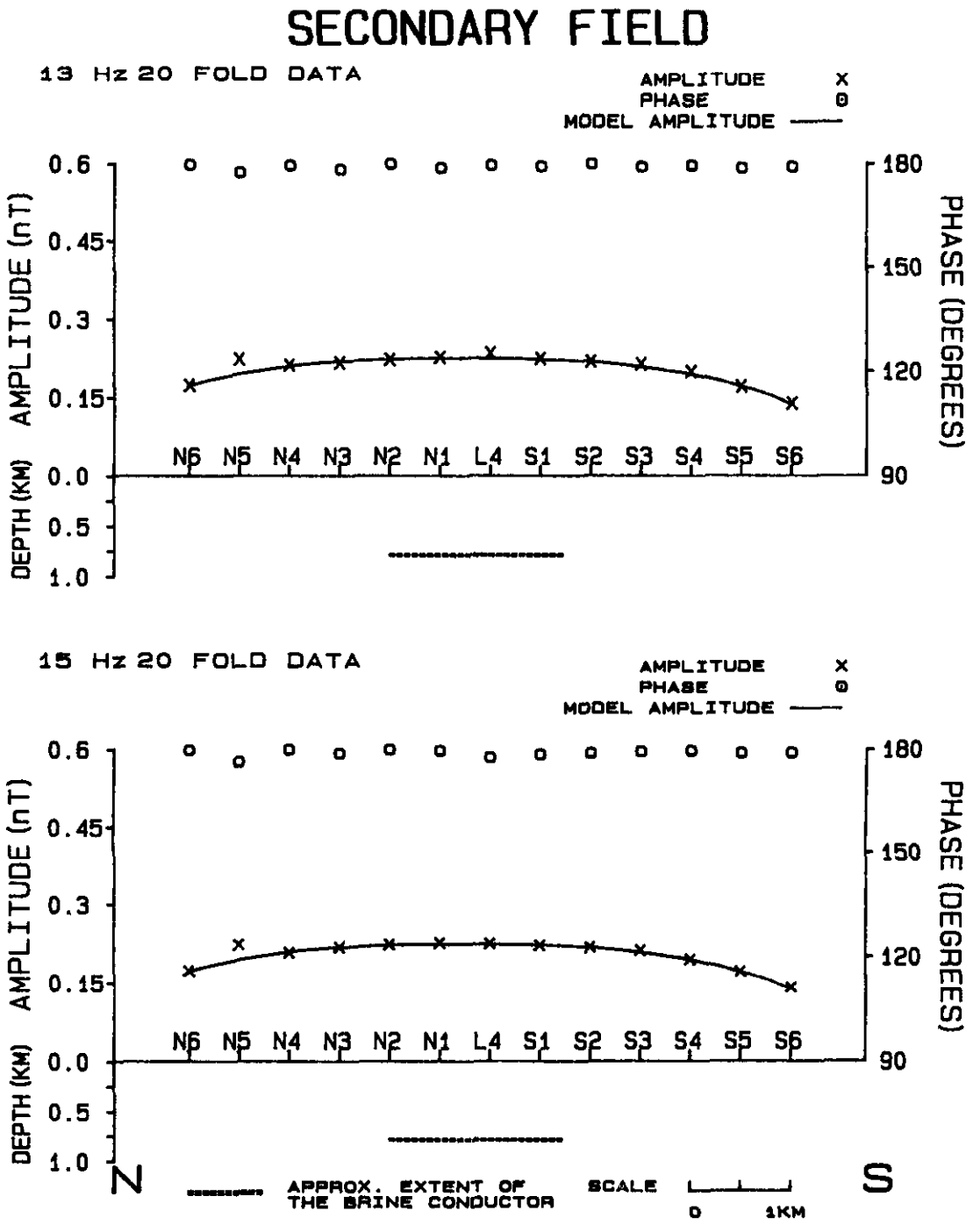

Fig. 9. At 13 and 15 Hz the localized anomalies were not present. The arched form of these profiles indicates that, at these frequencies, only a reflected image of the primary field was being detected.

lies. The best example of such an anomaly is shown by the 5-Hz data (Figure 7). However, the noise level in the phase data was found to be too severe to allow a good fit to be achieved, as can be seen in the examples for 5 and 9 Hz shown in Figure 10. This level of noise indicates that the method of retrieving absolute phase from relative phase between the vertical and horizontal components was not as effective as anticipated. Accordingly, the system has now been developed to permit direct measurement of absolute phase. This can now be accomplished by taking simultaneous, synchronized digital records of both the detected field and the transmitter-output waveform.

An unusual characteristic of the profiles in Figures 6 to 9 is that the anomalies display the character of typical vertical-component anomalies, yet these are profiles of total secondary field. A total-field anomaly over an isolated line current would be a single positive peak located directly over the line current. However, when the field of a line current is combined with a stronger regional field which has no horizontal component, then the resulting total-field vector shows characteristics which are dominated by the vertical component of the line current field. This effect is shown in Figure 11 where the field due to a horizontal line current is presented in the form of its vertical and horizontal components and the total field which results from the vector combination of those two components. The total-field profile was calculated for 5 cases in which a DC bias was added to the vertical component of the line current field. This bias was increased in steps of 25 percent of the peak total field which existed before any bias was applied. Each total-field profile has been plotted with the baseline displaced downwards to allow the transformation of the profile to be more easily appreciated. With a 25 percent bias, the total-field profile lost the symmetric form which it displayed for zero bias. At 100 percent bias, the total field displayed a form which was a quite close approximation to the form shown by the vertical-component profile.

Thus, the vertical-component anomaly form, seen in the recorded data, was due to the combination of the fields from the brine conductor with the strong background image field of the transmitter reflected from the conductive environment. The image field was a predominantly vertical field at each station, as was the primary field.

The positions of the currents C1 and C2 in Figures 6 to 9 do not correspond exactly to the lateral position of the oil field, but their separation is comparable with the width of the field. This width comparison suggests that these currents are associated with the edges of the brine conductor. Their displacement may be due to the position of the transmitter with respect to the conductor. If the transmitter had been located to the west of the survey line it is possible that a displacement of these current positions to the north would have been seen, rather than the southerly displacement observed with the transmitter to the east.

An alternative explanation of this apparent southerly displacement of C1 and C2 may lie in the fact that the known extent of the oil field and the extent of the sandstone lens, which created the structure which traps the oil, are not identical. In addition, electric logs of the available exploration drill holes indicate that major changes in the conductivity of the sandstone occur laterally and these are not related to the location of the oil at the top of the structure. Thus, the displacement observed is not unrealistic if C1 and C2 were confined within the most conductive part of the sandstone lens, the location and extent of which is not as well-defined as the extent of the oil field.

Figure 10 presents both amplitude and phase profiles for the 5- and 9-Hz cases along with the matching profiles. The magnitudes and phases of the currents used to generate the matching profiles are shown below each set of profiles. Current C4 was omitted from the 5-Hz profile match to illustrate that the currents which were introduced close to the ends of the traverse provided only a marginal improvement in the match to the observed data. Currents C3 and C4 cannot be viewed as being geologically real unless the traverse is extended to provide full development of these suggested anomalies.

The relative magnitudes and phases of the matching currents in Figure 10 show that, at both 5 and 9 Hz, current C1 was stronger than C2 but that they had the same polarity. If the current gathered into the conductor had been due to direct induction alone, then it would have formed a horizontal vortex which would have followed the perimeter of the brine conductor. This would have resulted in currents of equal magnitude but exactly opposite polarity being associated with the north and south edges of the conductor. If any current had been gathered into the brine conductor from the host rock it would have had a single direction of flow within the conductor. Thus, a gathered current would have added to the directly induced current along one edge of the conductor while opposing the directly induced current along the other edge. If the currents C1 and C2 are associated with the brine conductor, then the fact that these currents are not equal suggests that C1 and C2 represent currents which were a combination of directly induced and gathered currents. The fact that C1 and C2 have the same polarity suggests that, in this case, the gathered currents overwhelmed the induced vortex.

In Figure 10, the magnitude of the currents needed to match the 5-Hz data was significantly greater than that needed for the 9-Hz data. This can possibly be ascribed to the gathered current becoming less effective at higher frequencies, as both the galvanic and the induced currents in the host environment were confined closer to the surface and were unable to reach the target conductor.

Thus, it appears that the following points can be made:

1. The results are compatible with the depth of the known brine conductor and appear to be associated with the known lateral position of that conductor, although the lateral extent of the brine is not as well known from drilling as is its depth.
2. The profiles have an unusual form, but this can be seen to be a logical and necessary consequence of the combi-

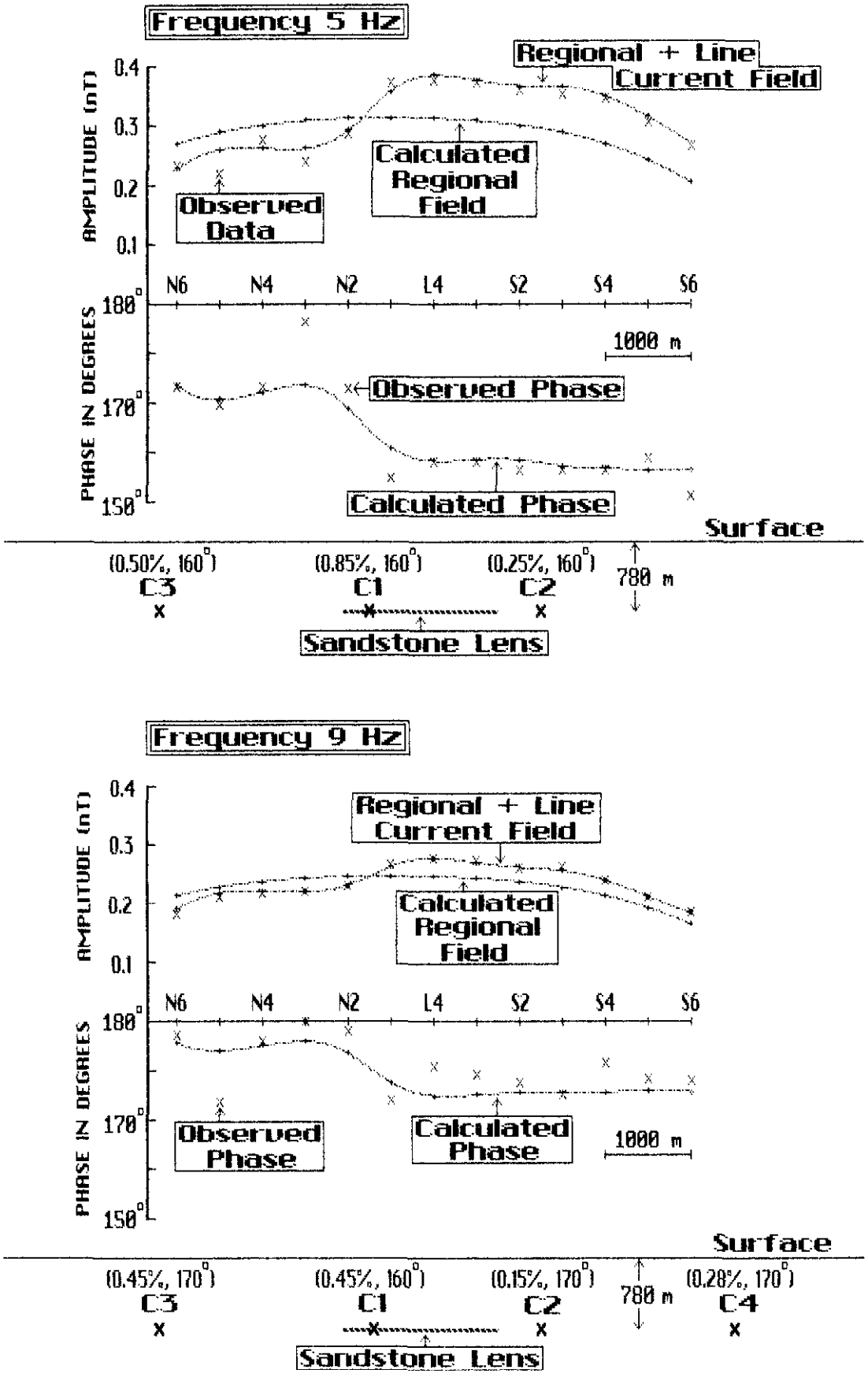

Fig. 10. Phase data for the localized anomalies was too noisy to permit good matches to be achieved.

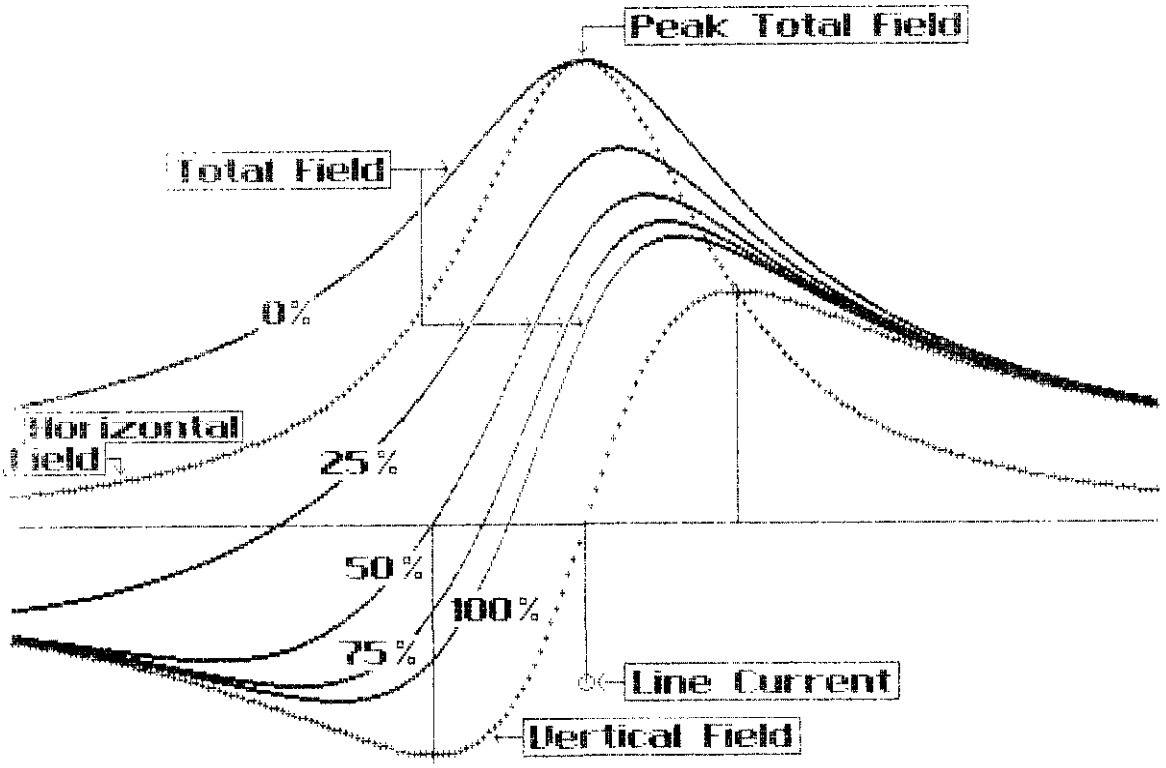

Fig. 11. The recorded profiles display the character of vertical-component profiles yet were actually total-field profiles. This illustration shows the transition of the total-field anomaly due to a line current from a single peaked form to a form which resembles the vertical component of the field as different levels of bias are added to the vertical component of the line-current field.

nation of fields from a deep-seated line current and a background field.

3. The loss of the anomalies at higher frequencies is consistent with the local anomalies having been generated by a deep-seated conductor which could not be reached by either the directly induced or the current-gathering effects at higher frequencies.
4. While the current magnitudes returned by the profile-matching process are not the actual magnitudes of the currents which flowed in the conductor, their relative magnitudes and polarities suggest that the currents within the conductor were dominantly gathered from the host environment.
5. The theoretical model used to match the observed data is limited and simplistic, but it showed that the known brine conductor is at least as likely as any other conductivity distribution to be the source of the observed anomalies. Of particular note is the fact that the model worked almost equally well at all frequencies despite the fact that the depth of the line currents was fixed at the known depth of the brine for all frequencies. Any attempt at a more sophisticated interpretation would need better phase data.

Discussion

This survey was conducted with a prototype system and the results have shown a clear need for development in some components of the system. However, even without these developments, the system provided results which strongly suggest that we did detect the David oil field conductor at a depth of 780 m in an environment with a 5 ohm-m resistivity.

The SQUID detector proved to be a very effective sensor for the low-frequency fields which were necessary for this survey. Operating along a traverse parallel to the line transmitter allowed the traverse to be long enough for the full development of the anomalies while not requiring dangerously large currents in the transmitter.

The survey required six days to complete with a crew of three people, but in more fully developed form the time required could be greatly reduced because the survey described here required a large number of tests which would not be needed in a fully developed system. This type of survey could provide a relatively low cost means of reconnaissance for brine-filled sand lenses and channels. The effective depth range for detecting such structures would be approximately 1 km.

Only a very limited frequency range was used in this survey because of the emphasis on detecting the conductor by lateral profiling. However, the recording system is capable of dealing with a frequency band from 0 to 5000 Hz so that a broad band of frequency data could be acquired at each station and could be inverted to a depth profile.

References

Bosschart, R.A., 1964, Analytical interpretation of fixed source electromagnetic prospecting data: Ph.D. thesis, Univ. of Delft, Holland.

Duckworth, K., 1972, Turam interpretation by curve matching using a line current approximation: Geophys. Prosp. **20**, 514-528.

_____, 1988, A modified current filament model for use in the interpretation of frequency domain electromagnetic data: J. Can. Soc. Expl. Geophys. **24**, 66-71.

_____ and Bays, A.R., 1984, A modified mode of operation for the Turam electromagnetic exploration system with benefits for deep exploration: Geophys. Prosp. **32**, 317-335.

_____ and Cummins, C., 1989, A physical scale model study of the comparative performance of two modes of operation for fixed loop Turam type electromagnetic systems: Geophys. Prosp., in press.

_____ and O'Neill, D., 1989, Turam responses for single and double conductor targets in a conductive host environment: Geophys. Prosp., submitted.

Jagodits, F.L., Betz, J.E., Krause, B.R., Saracoglu, N. and Wallis, R.H., 1986, Ground geophysical surveys over the McClean uranium deposits, northern Saskatchewan: Can. Inst. Min. Bull. **79**, 35-50.

Keller, G.F. and Frischknecht, F.C., 1966, Electrical methods in geophysical prospecting: Pergamon Press, Inc.

Lajoie, J.J. and West, G.F., 1976, The electromagnetic response of a conductive inhomogeneity in a layered earth: Geophysics **41**, 1133-1156.

Parkhomenko, E.I., 1967, Electrical properties of rocks (trans. G.V. Keller): Plenum Press.

Vrba, J., Fife, A.A. and Burbank, M.B., 1981, Digital SQUID electronics in geophysical applications: *in* Weinstock, H. and Overton, W.C., Eds., SQUID applications to geophysics: Soc. Expl. Geophys.

Zimmerman, J.E. and Campbell, W.H., 1975, Tests of cryogenic SQUID for geomagnetic field measurements: Geophysics **40**, 269-284.